STUDY OF THE MOTION STABILITY AND OPERATIONAL SMOOTHNESS OF AN AGRICULTURAL ROBOTIC PLATFORM

/

ԳՅՈՒՂԱՏՆՏԵՍԱԿԱՆ ՆՇԱՆԱԿՈՒԹՅԱՆ ՌՈԲՈՏ-ՀԱՐԹԱԿԻ ՇԱՐԺՄԱՆ ԿԱՅՈՒՆՈՒԹՅԱՆ ԵՎ ԸՆԹԱՑՔԻ ՍԱՀՈՒՆՈՒԹՅԱՆ ՈՒՍՈՒՄՆԱՍԻՐՈՒԹՅՈՒՆ

Arshaluys TARVERDYAN[1)], Aghavard KHACHATRYAN[2)], Artur ALTUNYAN[1*)], Sergey PAPYAN[1)], Albert GRIGORYAN[1)]

[1)]Scientific Research Institute for Agricultural Mechanization and Automation, Armenian National Agrarian University, Yerevan, Armenia

[2)]Chair of Higher Mathematics and Physics, Armenian National Agrarian University, Yerevan, Armenia

Tel: +37455327325; E-mail: arturaltunyan@gmail.com

Corresponding author: Artur Altunyan

DOI: https://doi.org/10.35633/inmateh-79-73

***Keywords:** movement smoothness, oscillation characteristics, robotic platform, stability on slopes, vehicle stability*

ABSTRACT

This study focuses on the development of a multifunctional agricultural robotic platform. Previous articles in this series established the need for such a platform based on the specific soil and climatic conditions of the Republic of Armenia. Tests of a laboratory prototype indicated the need for further investigation of the platform's dynamic behavior, particularly during operation in orchards and agricultural fields on sloping terrain, which is common in Armenia. Particular attention was given to changes in platform inclination during turning maneuvers on slopes and to the yaw moment generated about the vertical axis in four-wheeled robotic platforms with independently controlled wheels. Based on a mathematical model of the chassis incorporating elastic elements (springs) and damping elements (shock absorbers), the differential equation governing the motion of the platform's center of mass was formulated, together with moment equations about the transverse and longitudinal axes passing through the center of mass. Analysis of these equations yielded the differential equations governing the platform's vertical oscillations. Expressions were subsequently derived for the displacement, velocity, acceleration, and jerk associated with the platform's free oscillations. These equations can be used to evaluate ride smoothness and determine the spring stiffness and shock-absorber damping coefficient required to achieve the desired suspension performance.

ԱՄՓՈՓԱԳԻՐ

Ներկայացվող հոդվածը նվիրված է գյուղատնտեսական բազմաֆունկցիոնալ ռոբոտ-հարթակի մշակման խնդրին: Շարքի նախորդ հոդվածներում հիմնավորվել է այդպիսի ռոբոտ-հարթակի մշակման անհրաժեշտությունը ելնելով հանրապետության հողակլիմայական պայմանների առանձնահատկություններից: Մշակվող ռոբոտ-հարթակի լաբորատոր փորձանմուշի փորձարկումները ցույց տվեցին, որ անհրաժեշտ է իրականացնել լրացուցիչ հետազոտություններ, որոնք հնարավորություն կտան բացահայտելու ռոբոտ-հարթակի շարժման դինամիկան հատկապես թեքություններում տեղակայված այգիներում ու դաշտերում, որոնք բնութագրական են Հայաստանի Հանրապետության հողատեսքերի համար: Հաշվի են առնվել թեքություններում շրջադարձի ընթացքում տեղի ունեցող թեքության անկյան տրանսֆորմացիան, և որ չափազանց կարևոր է, միայն քառանիվ, իրարից անկախ կառավարվող անիվներով ռոբոտ-հարթակներին ներհատուկ, ուղղաձիգ առանցքի շուրջ առաջացող պտտող մոմենտը, որը էական ազդեցություն է թողնում կայունության վրա: Ընթացքային մասի, առաձգական էլեմենտ (զսպանակ) և մարիչ (ամորտիզատոր) պարունակող հաշվարկային սխեմայի համար կազմվել են ռոբոտ-հարթակի մասսաների կենտրոնի շարժման դիֆերենցիալ հավասարումը, ծանրության կենտրոնով անցնող լայնական ու երկայնական սիմետրիայի առանցքների նկատմամբ մոմենտների հավասարումները, դրանց վերլուծության արդյունքում ստացվել են հարթակի ուղղաձիգ տատանումների դիֆերենցիալ հավասարումները: Արդյունքում ստացվել են հարթակի սեփական տատանումների ընթացքում առաջացող տեղափոխությունների, արագությունների, արագացումների և արագացումների փոփոխության որոշման հավասարումները, որոնք հնարավորություն են տալիս գնահատելու ընթացքի սահունությունը և որոշելու դրա ապահովման համար անահրաժեշտ կախոցի համակարգի զսպանակի անհրաժեշտ կոշտությունն ու ամորտիզատորի դիմադրության գործակիցը:

INTRODUCTION

In all countries ensuring food security has always been, and remains, one of the most pressing challenges facing agricultural production. The solving of this problem must involve the conservation and improvement of land resources, meeting environmental requirements, increasing production volumes, the production of environmentally friendly food products, full mechanization of agricultural production, and, particularly importantly, reducing of the energy intensity of these processes. It is evident that the stated problem is multidimensional, and its complete solution using existing technologies and technical means is objectively limited (*Abrosimov and Raykov, 2022; Bak and Jakobsen, 2004; Fontani et al., 2025; O'Meara, 2019; Ritchie, 2024*).

For this reason, two key trends have recently become central to agricultural production technological processes (*Abrosimov and Raykov, 2022; Markets and Markets, 2025; Navone et al., 2025; Tarverdyan et al., 2025*).

First, one of the fastest growing areas in recent years in agricultural production is precision and digital technologies in crop and livestock production.

Second, the direction without which it is impossible to effectively utilize and implement the information obtained through the above-mentioned technologies is the organization of robot-assisted agricultural production. This implies that the development and large-scale implementation of robotics play a central role in addressing the stated problem (*Abrosimov and Raykov, 2022; Navone et al., 2025; O'Meara, 2019; Ritchie, H., 2024)*.

Although the global agricultural robotics market is developing at an unprecedented rate (over the last five years alone, its volume has increased approximately 20-fold) (*Bak and Jakobsen, 2004; MarketsandMarkets, 2025*), the application of such systems in the agricultural sector of the Republic of Armenia remains highly limited. This is primarily due to their relatively high market price, making them inaccessible to the majority of local producers, and second, to their structural characteristics, which result in low operational reliability under the soil conditions of the Republic of Armenia (*Tarverdyan et al., 2025*).

It follows that the problem can be addressed through two approaches: either partial structural modifications should be made to existing robots, or a new universal robotic platform should be developed that is better adapted to the country's soil conditions (presence of stones of various sizes, fragmented terrain) and, importantly, is cost-effective.

For all mobile agricultural robots, the mobile platform is a critical component that plays a key role in the overall system performance of the system. It is therefore not surprising that researchers in this field have devoted significant efforts to the development of high-performance mobile platforms for agricultural robots, as well as to improving their control and positioning accuracy, since these issues are of crucial importance in precision agriculture (*Amin et al., 2025; Bayar et al., 2015; Lipiński et al., 2016; Qiu et al., 2018; Zagazezheva and Berbekova, 2021*).

The operational practice of agricultural robotic platforms over the last 20–25 years, as well as the results of numerous research studies, lead to a clear conclusion: from the perspective of accurate perception and response to external influences during agro-technological processes, minimal energy consumption, minimal soil damage, and high maneuverability, four-wheeled robotic platforms are preferred (*Akimov, 2017; Blasco et al., 2002; Cho et al., 2002*).

In addition, four-wheeled robotic platforms with independently controlled wheels provide high maneuverability and enable parallel motion of the vehicle during turning, allowing positional accuracy and orientation accuracy to be controlled independently (*Bak and Jakobsen, 2004; Cho et al., 2002; Orebäck and Christensen, 2003; Tarverdyan et al., 2025*).

Research on robotic platforms is primarily driven by the shortcomings and challenges identified during their operation. Current studies place significant emphasis on optimal control, stability, and ensuring smooth motion. In this regard, the studies conducted by a group of researchers are of particular interest *(Blasco et al., 2002; Fountas et al., 2020; Zakaria et al., 2024*), in which the authors demonstrate that integrated control systems (ICS)—such as combined steering and wheel torque control, suspension and wheel torque coordination, as well as the integration of steering control systems with suspension—provide superior performance characteristics for multi-axle mobile devices (Multi-axle Vehicles, MAV) compared with skid-steering control systems (SCS). In this optimal distribution approach, the target vehicle forces and yaw torque are distributed among the individual tire forces (*Ali et al., 2017; Li and Shi, 2017; Zakaria et al., 2024*).

Another group of researchers has approached the problem from the perspective of determining the critical speed and its more accurate estimation for a two-axle dynamic model. A 4×2-wheel configuration was adopted as the vehicle model, and the acting forces and other lateral dynamic parameters were calculated for this model. The problem was analyzed in terms of the forces acting on the vehicle during turning and on inclined surfaces to ensure stability, taking into account the redistribution of reaction forces and variations in the tire–surface adhesion coefficient (*Ivanov et al., 2025*).

In a previous study devoted to this problem (*Tarverdyan et al., 2025*), the kinematic parameters of the motion subsystem of a robotic platform were examined in detail. In particular, the relationships between four independently steerable wheels, steering angles, and their angular velocities were established. Lateral forces arising during turning on a horizontal plane were also partially analyzed.

The present article is devoted to the investigation of the stability of robotic platform motion and conditions of lateral slip on sloped terrain, as well as to the assessment of motion smoothness based on the proposed model.

MATERIALS AND METHODS

Stability of Robotic Platform Motion on Inclined Surfaces

As previously noted, for robotic platforms intended to perform agro-technological operations, the four-wheel configuration with independently controlled wheels is considered preferable. The ability of the platform to perform parallel translational motion, in some cases without rotational turning, provides high maneuverability.

Independent control of all four wheels minimizes lateral slip, thereby reducing not only soil disturbance but also the wear of drivetrain components (*Bak and Jakobsen, 2004; Torii, 2000*).

Although the dynamics of a four-wheeled independently controlled system are inherently nonlinear and control is not straightforward, relatively simple control systems can still be effective at low operational speeds (2–6 km/h), (*Cho et al., 2002; MarketsandMarkets, 2025; Tarverdyan et al.,2025*). The conceptual scheme of the proposed robotic platform is presented in Figure 1. It consists of a platform frame (1), on which various agro-technological implements and devices are mounted; four drive wheels with independent actuation (2); a wheel steering control unit (3); and a wheel steering mechanism (4).

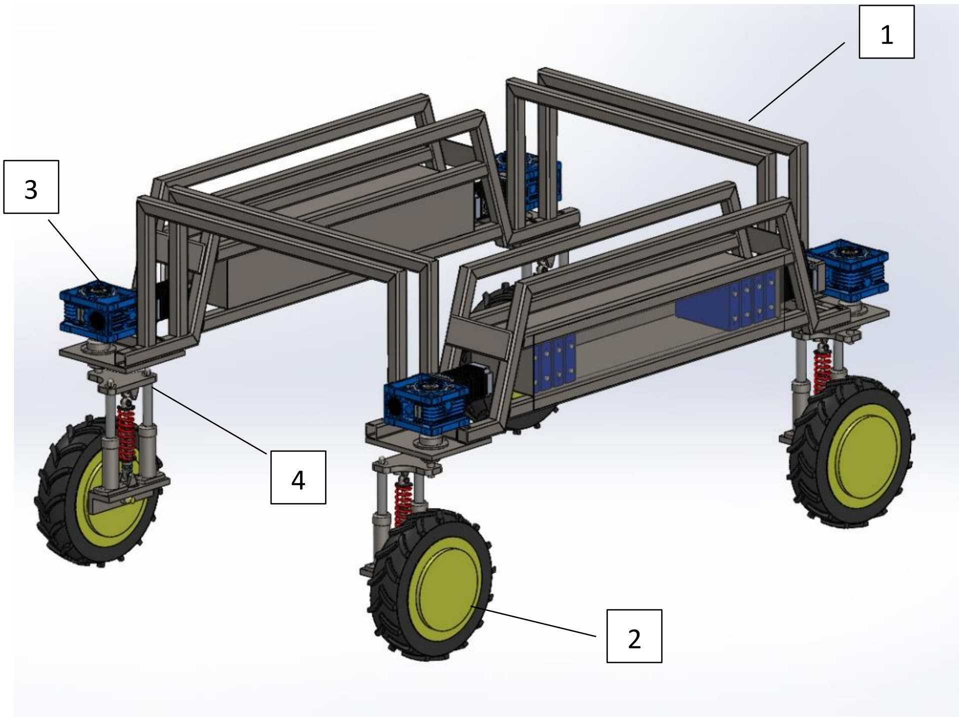

Fig. 1 - 3D model of the developed robotic platform

A detailed kinematic analysis of the locomotion subsystem of the developed robotic platform (*Tarverdyan et al., 2025*) yielded equations that make it possible to determine and refine the parameters used as the basis for programming the platform's turning motion on a horizontal surface.

As a result of the dynamic analysis, precise equations for determining lateral slip forces were obtained. These equations enable the development of a robotic platform drivetrain in which wheel slip during turning is minimized, thereby minimizing soil damage while ensuring operational reliability and durability (*Tarverdyan et al., 2025*).

An agricultural robotic platform can also perform agro-technological operations in fields located on sloped terrain, which is particularly characteristic of the Republic of Armenia. Under such conditions, during the development of the robotic platform, the issue of motion stability, especially during turning, becomes a key subject of analysis.

Assume that the robotic platform performs a turning maneuver on a planar slope inclined at an angle β where the rotation axis OO' is perpendicular to the inclined plane and is positioned upslope relative to the robotic platform (Figure 2). The geometric dimensions of the platform are – width B and length L. Since the goal is to develop a structure that is as symmetric as possible in terms of both geometry and mass distribution, it can be assumed that the center of mass coincides with point O_1', located at the intersection of the longitudinal (x_2) and transverse (y_2) symmetry axes of the platform. In this case $a = \frac{L}{2}, b = \frac{B}{2}$. Let the distance of the center of mass from the supporting plane CDEF be denoted by h, and the turning radius of the center of mass by R_0. The steering angles of the wheels are $\theta_1, \theta_2, \theta_3, \theta_4$, while the corresponding turning radii are R_1, R_2, R_3, R_4.

Let consider the turning motion of the robotic platform with a constant turning radius on a slope inclined at an angle β (Figures 2 and 3). Before determining the forces and reactions acting on the platform, it is necessary to account for the transformation of the slope inclination during rotational motion, since it directly affects the magnitude of the force components involved. Let the coordinate system xoy (Figure 3) be fixed to the inclined plane, where the y-axis is aligned with the transverse direction of the slope and the x-axis with the longitudinal direction, with the origin located at the center of rotation. When the rotation angle is φ = 0 (position $\mathcal{A}$ of the robotic platform), the transverse symmetry axis y_1 of the robotic platform coincides with the y-axis, the longitudinal axis (x_1) inclination angle is β.

When φ = 90°, the axis x_1 becomes parallel to the y-axis $x_1 \parallel y$, while y_1 coincides with the x-axis and is inclined at angle β (Figure 2). When φ = 180°, the configuration becomes symmetric to position $\mathcal{A}$. For all intermediate positions (e.g., position B), the inclination of the robotic platform is characterized by angles β_1 and β_2, which are determined as follows:

$$\begin{cases} sin\beta_1 = sin\beta \cdot sin\varphi, \\ sin\beta_2 = sin\beta \cdot cos\varphi. \end{cases} \tag{1}$$

Let consider the analysis of the forces acting on the robotic platform during turning motion at an arbitrary intermediate position B within the range $0 \le \varphi \le 90^0$ (Figure 3) (within the interval $90 - 180^0$, the configuration is repeated symmetrically).

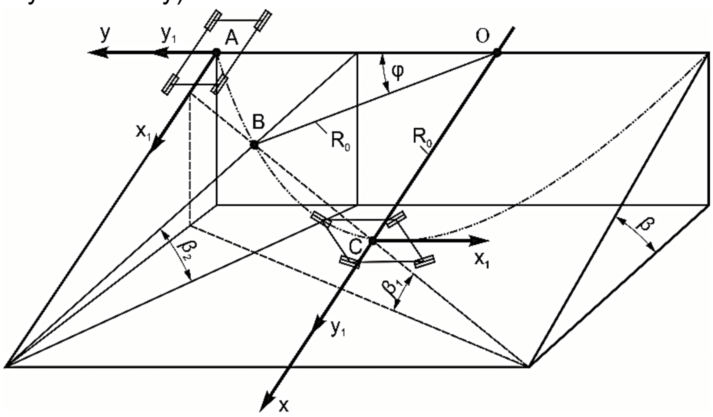

Fig. 2 - Schematic diagram of tilt-angle transformation during the turning motion of the robotic platform

At the specified position, the following forces and torques act on the robotic platform:

The gravitational force G acts at the center of mass and has three components: $G_x = G\cos\beta_1 \cdot sin\beta_2$, directed along the x_2 axis, $G_y = Gsin\beta_1$ - directed along the y_2 axis, $G_z = G\cos\beta_1 \cdot \cos\beta_2$ – perpendicular to the inclined plane.

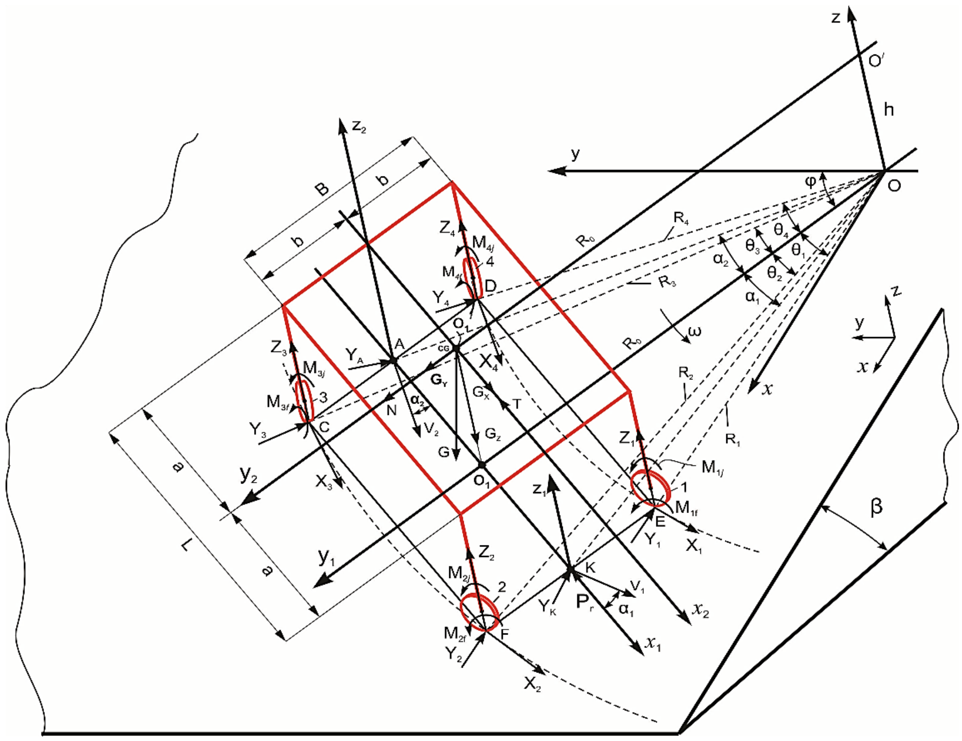

Fig. 3 - Kinematic and dynamic analysis scheme of the turning motion of the robotic platform on an inclined surface

At the wheel–ground contact surfaces, the support reactions Z_i, act normal to the supporting surface. The driving (tractive/tangential) forces Xi act at the wheel contact surfaces and are perpendicular both to the wheel radii (r_w) and to the turning radii R_i associated with rotation about point *O*. The lateral slip resistance forces Y_i, also act at the wheel–ground contact surfaces and are directed along the turning radii (R_i). In the general case, the wheels are also subjected to a torque of the rolling resistance (M_{if}).

The robotic platform is additionally subjected to inertial force factors. At the center of mass (O_1'), the longitudinal inertial force T acts along the x_2 axis, with its direction determined by the nature of the motion (acceleration or deceleration). The centrifugal force N associated with curvilinear motion acts along the y_2 axis. The wheels are also subjected to inertial torques (M_{ij}), as well as the inertial torque of the robotic platform associated with curvilinear motion about the z-axis, denoted by M_j (*Litvinov, 1971; Qiu et al., 2018; Zinoviev, 1975*).

To solve the problem of lateral slip of the robotic platform, it is first necessary to determine the support reactions at the wheel–ground contact surfaces, namely Z_1, Z_2, Z_3 *and* Z_4. By formulating the equilibrium equations with respect to the axes passing through the wheel support points (CD, EF, CF and DE) and performing the corresponding transformations, the following equations are obtained:

$$Z_1 + Z_2 = \frac{G_z}{2} + \frac{G_x \cdot h}{2a} - \frac{T \cdot h}{2a} - \frac{4M_{ij}}{2a} \tag{2}$$

$$Z_3 + Z_4 = \frac{G_z}{2} - \frac{G_x \cdot h}{2a} + \frac{T \cdot h}{2a} + \frac{4M_{ij}}{2a} \tag{3}$$

$$Z_1 + Z_4 = \frac{G_z}{2} + \frac{G_y \cdot h}{2b} - \frac{N \cdot h}{2b} \tag{4}$$

$$Z_2 + Z_3 = \frac{G_z}{2} + \frac{G_y \cdot h}{2b} + \frac{N \cdot h}{2b} \tag{5}$$

Besides:

$$Z_1 + Z_2 + Z_3 + Z_4 = G_z \tag{6}$$

Let's also introduce the following denotations:

$$\begin{cases} Z_1 + Z_2 = \mathcal{A} \\ Z_3 + Z_4 = B \\ Z_1 + Z_4 = C \\ Z_2 + Z_3 = \mathcal{D}. \end{cases} \Rightarrow \mathcal{A} + B = C + \mathcal{D} \tag{7}$$

Let us denote: $Z_1 = S$, where S is an arbitrary parameter. Then:

$$\begin{cases} Z_1 = S \\ Z_2 = \mathcal{A} - S \\ Z_3 = B - C + S = \mathcal{D} + S \\ Z_4 = C - S. \end{cases} \tag{8}$$

The parameter S characterizes the redistribution of the load among the supports, which does not alter the quantities $(Z_1 + Z_2)$, $(Z_1 + Z_4)$, $(Z_3 + Z_4)$ and $(Z_2 + Z_3)$, in other words, equilibrium is preserved, and the model is self-balancing (*Buchholz, 2023; Ilarionov, 2013; Litvinov, 1971*).

Using Equations (2), (3), (4), and (5), together with relations (6) and (8), and considering that $G_x = G\cos\beta_1 \cdot sin\beta_2$, $G_y = Gsin\beta_1$, $G_z = G\cos\beta_1 \cdot \cos\beta_2$, where the angles β_1 and β_2 are determined from Equation (1), $N = \frac{G}{g}\omega^2 R_0$, $T = \frac{G}{g} \cdot \frac{dv}{dt}$, $M_{ij} = J_w \cdot \frac{d\omega_w}{dt}$ (J_w is the wheel torque of inertia, and $\frac{d\omega_w}{dt}$ is the angular acceleration of the wheel), and taking into account that uniform motion of the robotic platform is considered, the following equations are obtained for the support reactions:

$$\left.\begin{aligned} Z_1 &= \frac{G}{4}cos\beta_1 \cdot cos\beta_2 - \frac{h \cdot G}{2L} \cdot sin\beta_1 + \frac{G \cdot h}{2B}cos\beta_1 \cdot sin\beta_2 - \frac{G \cdot h \cdot \omega^2 R_0}{g \cdot L} \\ Z_2 &= \frac{G}{4}cos\beta_1 \cdot cos\beta_2 + \frac{G \cdot h}{2L} \cdot sin\beta_1 + \frac{G \cdot h}{2B}cos\beta_1 \cdot sin\beta_2 + \frac{G \cdot h \cdot \omega^2 R_0}{g \cdot L} \\ Z_3 &= \frac{G}{4}cos\beta_1 \cdot cos\beta_2 + \frac{G \cdot h}{2L} \cdot sin\beta_1 - \frac{G \cdot h}{2B}cos\beta_1 \cdot sin\beta_2 + \frac{G \cdot h \cdot \omega^2 R_0}{g \cdot L} \\ Z_4 &= \frac{G}{4}cos\beta_1 \cdot cos\beta_2 - \frac{G \cdot h}{2L} \cdot sin\beta_1 - \frac{G \cdot h}{2B}cos\beta_1 \cdot sin\beta_2 - \frac{G \cdot h \cdot \omega^2 R_0}{g \cdot L} \end{aligned}\right\}. \tag{9}$$

It should be noted that the obtained solutions satisfy condition (7) and correctly reflect the physical nature of the problem.

Assessment and improvement of the Motion Smoothness of the Robotic Platform

Ensuring the smooth motion of the developed robotic platform is an important issue, since it directly determines the accurate execution of agro-technical processes, the operational reliability and durability of its components—particularly the suspension system—and the reliable performance of the orientation and control system.

Figure 4. shows the schematic diagram of the suspension system of the developed robotic platform, which includes an elastic element (spring) (1), a coaxially mounted hydraulic damper (shock absorber) (2), pneumatic wheels (3) each equipped with an independent electric hub motors, and an independent wheel steering control unit (4).

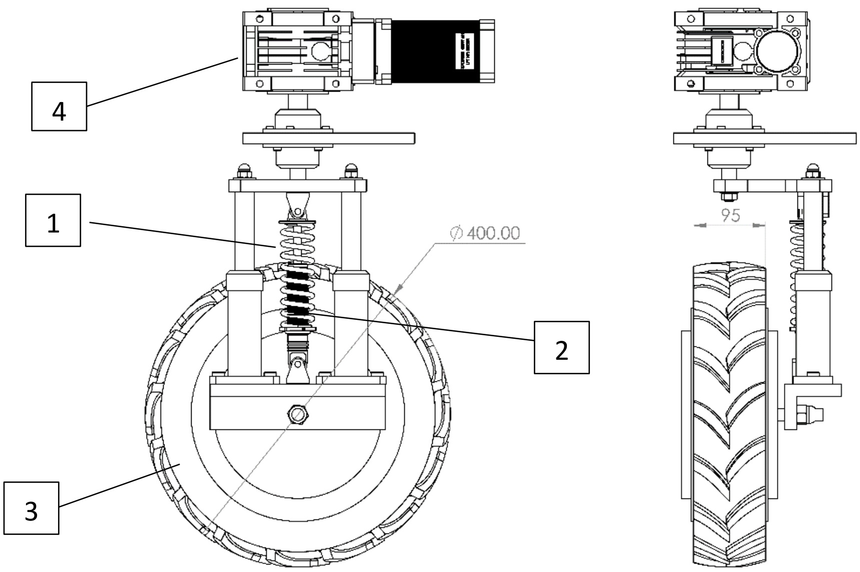

Fig. 4 - Schematic diagram of the suspension system of the robotic platform (all dimensions in *mm*)

It should be noted that, based on the presented suspension system configuration, from an application standpoint it is important to analyze the vertical translational oscillations of the platform, as well as the angular oscillations in the longitudinal and transverse symmetry planes.

The computational scheme of the problem is presented in Figure 5.

The data required for solving the problem are as follows:

- the overall dimensions of the robot platform: length L, width B;
- the identical stiffness of all four suspension springs c_s;
- wheel stiffness c_w;
- the sprung mass of the robotic platform M;
- the mass of the assemblies located below the springs (unsprung mass) m;
- the damping coefficient of the shock absorbers *k.* Since the two elastic elements the suspension spring and the wheel are connected in series, their combined stiffness can be represented by a single equivalent stiffness coefficient (*Ilarionov, 2013; Litvinov, 1971*).

$$c = \frac{c_s \cdot c_w}{c_s + c_w}.$$

Several assumptions were adopted in solving the problem, which considerably simplify the analysis while having no significant influence on the results.

It is assumed that the robotic platform moves uniformly across field surface irregularities, with the wheels continuously rolling over them while maintaining uninterrupted contact with the ground. Under these conditions, the wheel axles undergo vertical displacements (q_i).

The self-weight of the robotic platform and the loads mounted on it are assumed to be distributed symmetrically with respect to the *x* and *y* axes, such that the center of gravity of the total mass coincides with the origin of the coordinate system (Figure 5).

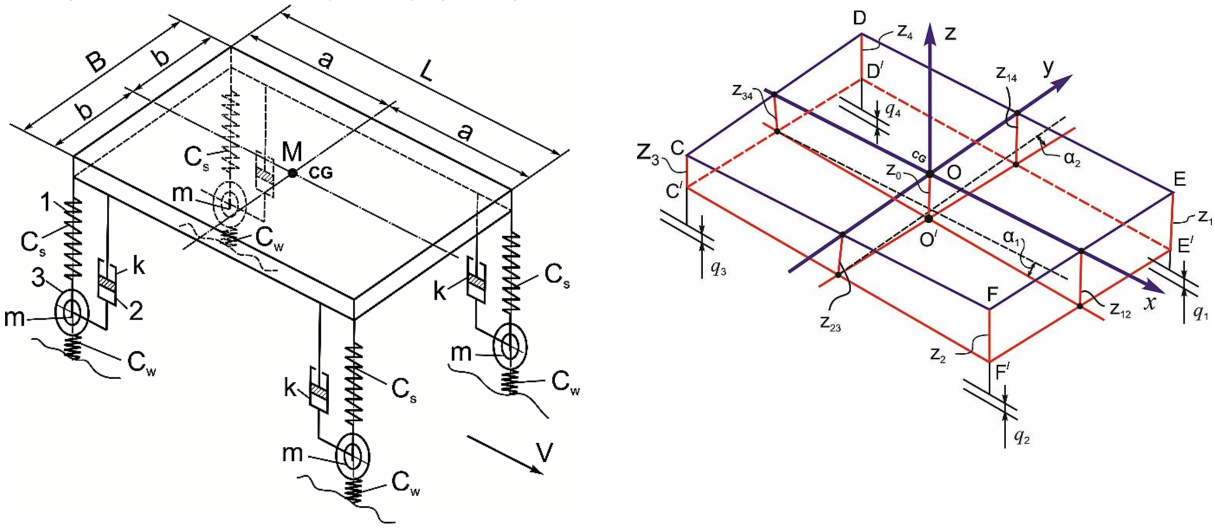

a) b)

Fig. 5 - Scheme for determining the driving/motion smoothness of the robotic platform:

a) schematic diagram of the suspension system,

b) computational scheme of the platform vertical displacements

In addition, the following notations were adopted:

z_0- vertical displacement of the platform's center of mass caused by oscillations;

z_1; z_2; z_3; z_4- vertical displacements of points C; D; E and F respectively located above the wheel axles;

α_1; α_2 – rotational angles of the platform in the longitudinal and transverse planes of symmetry, respectively;

a - distances from the front (conventionally defined) and rear wheel axles to the y-axis of symmetry passing through the center of mass (a=L/2, since the robotic platform is designed to have a symmetric structure);

b- distance from the wheel suspension attachment points to the x-axis of symmetry passing through the center of mass ($b = \frac{B}{2}$);

ρ_1- radius of inertia of the robotic platform with respect to the y-axis;

ρ_2- radius of inertia of the robotic platform with respect to the x-axis.

It is evident that the solution of the problem involves six unknowns: z_1; z_2; z_3; z_4; z_0 and α_1 (in one case) and α_2 (in the other case). In such situations, it is useful to establish relationships among these unknowns. Considering the sprung part of the robotic platform as a rigid horizontal plate CDEF (Figure 5), as a result of its vertical linear oscillations, at an arbitrary instant it will occupy the position Ć D́ É F́ while remaining planar. In the general case of oscillations, it is assumed that the displacements at the indicated points above the wheel axles are different, namely z_1; z_2; z_3; z_4. Under these conditions, geometric relationships exist between these displacements, making it possible to simplify the solution of the problem. In the longitudinal plane of symmetry of the robotic platform (along the x-axis), the displacements of the front edge points, as the midlines of the corresponding rectangles, are expressed as $z_{12}=\frac{z_1+z_2}{2}, z_{34}=\frac{z_3+z_4}{2}$. From the scheme shown in Figure 5, it follows that:

$$z_{12}=z_0+\alpha_1 \mathrm{a}\,, \qquad z_{34}=z_0-\alpha_1 \mathrm{a} \tag{11}$$

From which:

$$\alpha_1=\frac{z_{12}-z_{34}}{L}=\frac{z_1+z_2-z_3-z_4}{2L}\,.$$

Similarly, in the plane of lateral symmetry (along the y-axis), the displacements and the rotation angle of the platform are given by:

$$z_{14}=z_0+\alpha_2\cdot \mathrm{b};\; z_{23}=z_0-\alpha_2\cdot \mathrm{b} \tag{12}$$

$$\alpha_2=\frac{z_{14}-z_{23}}{B}=\frac{z_1+z_4-z_2-z_3}{2B}. \tag{13}$$

From the scheme, the following relationships also hold: $z_0=\frac{z_1+z_3}{2}$, $z_0=\frac{z_2+z_4}{2}$, from which it follows that:

$$\left.\begin{array}{c} z_2+z_3=z_2+z_4 \\ z_0=\dfrac{z_1+z_2+z_3+z_4}{4} \end{array}\right\} \tag{14}$$

To formulate the equations of motions for the considered problem, the principles of rigid-body dynamics are applied (*Biderman, 1980; Buchholz, 2023; Zinoviev, 1975*).

Since in this stage the task is to study only the free oscillations of the robotic platform, the forces caused by terrain irregularities, which include terms proportional to q_i, can be neglected as external excitations. In this case, the differential equation of motion of the platform's center of inertia can be written in the following form:

$$M\frac{d^2z_0}{dt^2}=\mathrm{k}\left(\frac{dz_1}{dt}+\frac{dz_2}{dt}+\frac{dz_3}{dt}+\frac{dz_4}{dt}\right)+c(z_1+z_2+z_3+z_4)=0. \tag{15}$$

The torque equations about the x and y axes passing through the center of inertia will be:

$$\mathrm{M}\rho_1^2\frac{d^2\alpha_1}{dt^2}+\mathrm{ka}\left(\frac{dz_1}{dt}-\frac{dz_2}{dt}-\frac{dz_3}{dt}+\frac{dz_4}{dt}\right)+c(z_1-z_2-z_3+z_4)=0, \tag{16}$$

$$\mathrm{M}\rho_2^2\frac{d^2\alpha_2}{dt^2}+\mathrm{k}b\left(\frac{dz_1}{dt}+\frac{dz_2}{dt}-\frac{dz_3}{dt}-\frac{dz_4}{dt}\right)+cb(z_1+z_2-z_3-z_4)=0. \tag{17}$$

By inserting the values of α_1, α_2 *and* z_0 from the Equations of (11); (13) and (14) in the Equations of (15); (16) and (17), the following is obtained:

$$\mathrm{M}\cdot\frac{1}{4}\left(\frac{d^2z_1}{dt^2}+\frac{d^2z_2}{dt^2}+\frac{d^2z_3}{dt^2}+\frac{d^2z_4}{dt^2}\right)+\mathrm{k}\left(\frac{dz_1}{dt}+\frac{dz_2}{dt}+\frac{dz_3}{dt}+\frac{dz_4}{dt}\right)+C(z_1+z_2+z_3+z_4)=0, \tag{18}$$

$$\frac{\mathrm{M}\rho_1^2}{2L}\cdot\left(\frac{d^2z_1}{dt^2}+\frac{d^2z_2}{dt^2}-\frac{d^2z_3}{dt^2}-\frac{d^2z_4}{dt^2}\right)+\ \mathrm{ka}\left(\frac{dz_1}{dt}-\frac{dz_2}{dt}-\frac{dz_3}{dt}+\frac{dz_4}{dt}\right)+\mathrm{ca}(z_1-z_2-z_3+z_4)=0, \tag{19}$$

$$\frac{\mathrm{M}\rho_2^2}{2B}\cdot\left(\frac{d^2z_1}{dt^2}+\frac{d^2z_4}{dt^2}-\frac{d^2z_2}{dt^2}-\frac{d^2z_3}{dt^2}\right)+\mathrm{kb}\left(\frac{dz_1}{dt}+\frac{dz_2}{dt}-\frac{dz_3}{dt}-\frac{dz_4}{dt}\right)+cb(z_1+z_2-z_3-z_4)=0. \tag{20}$$

To establish the relationships between Equations (18) and (19), (18) and (20) Equation (18) is multiplied by a and is added to (19), then (18) is multiplied by a and (19) is subtracted. In both cases, the resulting equations are divided by L. Similarly, Equation (18) is multiplied by *b* and added to Equation (20), and the resulting equation is divided by *B*. Equation (18) is then multiplied by *b* and Equation (20) is subtracted from the result, after which the resulting equation is divided by B. Considering the symmetry of the system, such that L=2a and B=2b, the following equations are obtained:

$$\mathrm{M}\left(\frac{\mathrm{a}^2+\rho_1^2}{2L^2}\right)\left(\frac{d^2z_1}{dt^2}+\frac{d^2z_2}{dt^2}\right)+\mathrm{M}\left(\frac{\mathrm{a}^2-\rho_1^2}{2L^2}\right)\cdot\left(\frac{d^2z_3}{dt^2}+\frac{d^2z_4}{dt^2}\right)+\mathrm{k}\left(\frac{dz_1}{dt}+\frac{dz_4}{dt}\right)+c(z_1+z_4)=0, \tag{21}$$

$$\mathrm{M}\left(\frac{\mathrm{a}^2-\rho_1^2}{2L^2}\right)\left(\frac{d^2z_1}{dt^2}+\frac{d^2z_2}{dt^2}\right)+\mathrm{M}\left(\frac{\mathrm{a}^2+\rho_1^2}{2L^2}\right)\cdot\left(\frac{d^2z_3}{dt^2}+\frac{d^2z_4}{dt^2}\right)+\mathrm{k}\left(\frac{dz_1}{dt}+\frac{dz_3}{dt}\right)+c(z_1+z_3)=0, \tag{22}$$

$$\mathrm{M}\left(\frac{\mathrm{b}^2+\rho_2^2}{2B^2}\right)\left(\frac{d^2z_1}{dt^2}+\frac{d^2z_4}{dt^2}\right)+\mathrm{M}\left(\frac{\mathrm{b}^2-\rho_2^2}{2B^2}\right)\cdot\left(\frac{d^2z_2}{dt^2}+\frac{d^2z_3}{dt^2}\right)+\mathrm{k}\left(\frac{dz_1}{dt}+\frac{dz_2}{dt}\right)+c(z_1+z_2)=0, \tag{23}$$

$$\mathrm{M}\left(\frac{\mathrm{b}^2-\rho_2^2}{2B^2}\right)\left(\frac{d^2z_1}{dt}+\frac{d^2z_4}{dt^2}\right)+\mathrm{M}\left(\frac{\mathrm{b}^2+\rho_2^2}{2B^2}\right)\cdot\left(\frac{d^2z_2}{dt^2}+\frac{d^2z_3}{dt^2}\right)+\mathrm{k}\left(\frac{dz_3}{dt}+\frac{dz_4}{dt}\right)+c(z_3+z_4)=0. \tag{24}$$

The Equations (21)–(22) and (23)–(24) are pairwise interrelated through their first and second terms Even in the particular case where $\mathrm{a}=\rho_1$ and $\mathrm{b}=\rho_2$, these interrelations are preserved. This indicates that the vertical oscillations of the considered robotic platform, characterized by the coordinates z_1; z_2; z_3 and z_4 are mutually coupled.

The following notation is introduced:

$$\mathrm{M}\left(\frac{\mathrm{a}^2+\rho_1^2}{2L^2}\right)=\mathrm{M}_1;\ \mathrm{M}\left(\frac{\mathrm{a}^2-\rho_1^2}{2L^2}\right)=\mathrm{M}_2;\ \mathrm{M}\left(\frac{\mathrm{b}^2+\rho_2^2}{2\mathrm{B}^2}\right)=\mathrm{M}_3;\ \mathrm{M}\left(\frac{\mathrm{b}^2-\rho_2^2}{2\mathrm{B}^2}\right)=\mathrm{M}_4.$$

The Equations (21) (22); (23) and (24) will take the following form:

$$\mathrm{M}_1\left(\frac{d^2z_1}{dt^2}+\frac{d^2z_2}{dt^2}\right)+\mathrm{M}_2\left(\frac{d^2z_3}{dt^2}+\frac{d^2z_4}{dt^2}\right)+k\left(\frac{d^2z_1}{dt}+\frac{d^2z_4}{dt}\right)+c(z_1+z_4)=0, \tag{25}$$

$$\mathrm{M}_2\left(\frac{d^2z_1}{dt^2}+\frac{d^2z_2}{dt^2}\right)+\mathrm{M}_1\left(\frac{d^2z_3}{dt^2}+\frac{d^2z_4}{dt^2}\right)+k\left(\frac{dz_2}{dt}+\frac{dz_3}{dt}\right)+c(z_2+z_3)=0, \tag{26}$$

$$\mathrm{M}_3\left(\frac{d^2z_1}{dt^2}+\frac{d^2z_4}{dt^2}\right)+\mathrm{M}_4\left(\frac{d^2z_2}{dt^2}+\frac{d^2z_3}{dt^2}\right)+k\left(\frac{dz_1}{dt}+\frac{dz_2}{dt}\right)+c(z_1+z_2)=0, \tag{27}$$

$$\mathrm{M}_4\left(\frac{d^2z_1}{dt}+\frac{d^2z_4}{dt^2}\right)+\mathrm{M}_3\left(\frac{d^2z_2}{dt^2}+\frac{d^2z_3}{dt^2}\right)+k\left(\frac{dz_3}{dt}+\frac{dz_4}{dt}\right)+c(z_3+z_4)=0. \tag{28}$$

The obtained equations enable to study the free oscillations of the robotic platform and also serve as a basis for the further investigation of its forced vibrations.

RESULTS AND ANALYSIS

Stability Conditions of the Robotic Platform Motion on Slopes

For the initial parameters of the developed robotic platform (L = 1.6m, B = 1.2m, G = 5000 N, h = 0.6m, ω = 0.278 s^{-1}, R_0 = 5m, β = 10^0) the following results are obtained for three characteristic positions using the derived equations:

when $\varphi=0^0$, $sin\beta_1=0$, $\beta_1=0$, $sin\beta_2=sin\beta$, $\beta_2=\beta$, $G_z=\mathrm{G}\cos\beta_1\cdot\cos\beta_2=5000\cdot0.9848=4925\,N$;

when $\varphi=45^0$, $sin\beta_1=sin\beta\cdot sin\varphi=0.1222$, $sin\beta_2=sin\beta\cdot cos\varphi=0.1222$, $cos\beta_1=cos\beta_2=0.9925$, $\mathrm{G_z}=\mathrm{G}\cos\beta_1\cdot\cos\beta_2=5000\cdot0.9925=4962.5\,N$;

when $\varphi=90^0$, $sin\beta_1=sin\beta\cdot sin\varphi$, $\beta_1=\beta$, $\beta_2=0$, $G_z=G\cos\beta_1\cdot\cos\beta_2=5000\cdot0.9848=4925\,N$;

Substituting the numerical values into Equations (9), the following values are obtained for the support reactions:

when $\varphi=0^0$, $Z_1=1355\,N$; $Z_2=1515\,N$; $Z_3=1095\,N$; $Z_4=960\,N$, verification: $Z_1+Z_2+Z_3+Z_4=4925\,N=\mathrm{G_z}$;

when $\varphi=45^0$, $Z_1=1195\,N$; $Z_2=1562.5\,N$; $Z_3=1265\,N$; $Z_4=940\,N$, verification: $Z_1+Z_2+Z_3+Z_4=4962.5\,N=\mathrm{G_z}$;

when $\varphi=90^0$, $Z_1=1004.5\,N$; $Z_2=1458\,N$; $Z_3=1458\,N$; $Z_4=1004.5\,N$, verification: $Z_1+Z_2+Z_3+Z_4=4925\,N=\mathrm{G_z}$.

The discussion of the robotic platform overturning problem is of little practical significance, since its operational speeds (3 – 6 km/h) and field slope angles (up to 7^0) cannot create a situation in which, even in the most unfavorable position ($\varphi=90^0$) the support reactions Z_1 and Z_4 become equal to 0. In this regard, the analysis of lateral skidding is of primary importance.

To determine the resistance forces against lateral skidding, it is first necessary to determine the tangential reactions (X_i) developed at all driving wheels during rolling motion. It is known that these reaction forces are determined as follows:

$$X_i = P - f\mathrm{Z}_i$$

where P is the circumferential force acting on each driving wheel, f is the rolling resistance coefficient, for various soils $f = 0{,}10 \div 0{,}25$ (*Cho et al., 2002; Litvinov, 1971*), while for cultivated soils $f = 0{,}25$; Z_i is the reaction force at the wheel–ground contact surface. For the considered case:

$$P = \frac{M_m \cdot i \cdot \eta}{r_w} - \mathrm{J}_w \cdot \frac{d\omega_w}{dt} \cdot \frac{1}{r_w}$$

where; r – wheel diameter, M_m - a torque developed by the electric motor, i – a transmission ratio of the motor–wheel drivetrain, η – a drivetrain efficiency, J – a wheel moment of inertia, $d\omega_w$ – an angular acceleration of the wheel

Taking into account that, $\frac{d\omega_w}{dt} = \frac{1}{r_w} \cdot \frac{dv}{dt}$ the following expression is obtained:

$$X_i = \frac{M_m \cdot i \cdot \eta}{r_w} - \mathrm{J}_w \cdot \frac{1}{r_w^2} \cdot \frac{dv}{dt} - f\mathrm{Z}_i \tag{29}$$

Under uniform motion conditions $\frac{dv}{dt} = 0$, therefore:

$$X_i = \frac{M_w}{r_w} - f\mathrm{Z}_i \tag{30}$$

In the case under consideration, where all four wheels are driving wheels and are independently controlled, the tangential (reaction) forces are not equal in either magnitude and direction. As a result, a torque M_z is generated, causing the robotic platform to rotate in the plane of motion. This torque significantly affects lateral skidding.

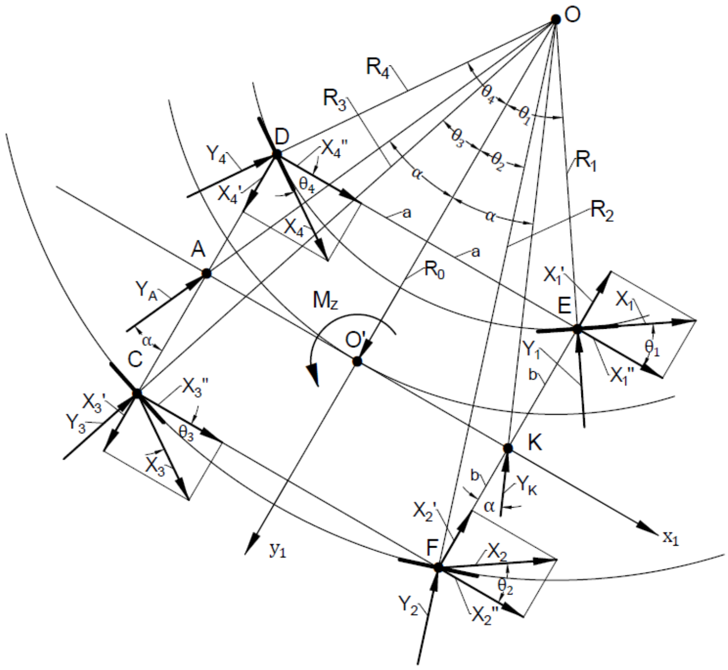

Fig. 6 - Schematic diagram for determining the torque about the vertical axis of the robotic platform

The value/magnitude of this torque is determined according to the scheme shown in Figure 6 as follows:

$$M_z = X_4' \cdot a + X_3' \cdot a + X_2' \cdot a + X_1' \cdot a - X_1'' \cdot b + X_2'' \cdot b + X_3'' \cdot b - X_4'' \cdot b,$$

$$M_z = (X_1 sin\theta_1 + X_2 sin\theta_2 + X_3 sin\theta_3 + X_4 sin\theta_4)a + (X_2 cos\theta_2 + X_3 cos\theta_3)b - (X_1 cos\theta_1 + X_4 cos\theta_4)b; \tag{31}$$

Taking into account that in the considered case $\theta_1 = \theta_4$; $\theta_2 = \theta_3$, for M_z Equation (32) becomes:

$$M_z = (X_1 + X_4)a \cdot sin\theta_1 + (X_2 + X_3)a \cdot sin\theta_2 + (X_2 + X_3)b \cdot cos\theta_2 - (X_1 + X_4)b \cdot cos\theta_1. \tag{32}$$

In the final equation, the forces X_1; X_2; X_3 and X_4 are determined by Equations (29) or (30). The problem of determining θ_1 and θ_2 as well as establishing the relationship between them, is comprehensively discussed in the work of *Tarverdyan et al. (2025)*. Therefore, the torque M_z is determined and for the indicated direction, it is always positive and at least equal to the sum of the first two terms of the equation.

After determining the force factors Z_i; X_i and M_z the lateral resistance (reaction) forces Y_1, Y_2, Y_3 and Y_4 can be determined. Naturally, these forces may be obtained from the dynamic equilibrium conditions of the robot platform; however, it should be emphasized that, in the analysis of the lateral drift phenomenon, the individual determination of these forces is not essential, since lateral skidding is caused by the pairwise combined lateral slip of the conventionally defined front and rear wheels. Proceeding from this consideration, the problem of determining the resultant forces (Y_3+Y_4) and (Y_1+Y_2) was examined.

Let the resultant force (Y_1+Y_2) be transferred to point K on the longitudinal axis of symmetry (x_2), and denote it by Y_K. Similarly, let the resultant $(Y_3+Y_4)=Y_{\mathcal{A}}$ be applied at point $\mathcal{A}$. It should be noted that this transfer does not alter the mechanical effect of the force system, since the forces Y_1 and Y_2; Y_3 and Y_4 form pairwise concurrent force systems. Since a symmetric system is considered, $Y_{\mathcal{A}}$ and Y_K are inclined relative to the $y_1-\text{axis}$ by the same angle α, where $tg\alpha=\frac{a}{R_0}$.

Considering the equilibrium condition of the torque of the forces acting on system with respect to the axes Z_1 and Z_2 passing through points $\mathcal{A}$ and K respectively, and using the schematic diagrams shown in Figures 3 and 6, the following equations are obtained:

$$\sum M_{Z_1}=0;\quad -Y_{\mathcal{A}}cos\alpha\cdot 2a+M_z+M_j+G_y\cdot a+N\cdot a=0;$$

$$\sum M_{Z_2}=0;\quad Y_K cos\alpha\cdot 2a+M_z+M_j-G_y\cdot a-N\cdot a=0;\quad \text{or}$$

$$Y_{\mathcal{A}}=\frac{M_z+M_j+G_y\cdot a+N\cdot a}{2a\cdot cos\alpha} \tag{33}$$

$$Y_K=\frac{N\cdot a+G_y\cdot a-M_z-M_j}{2a\cdot cos\alpha} \tag{34}$$

In these equations, the torque M_z is determined from Equation (32). The inertial torque M_j is determined as follows:

$$M_j=m\rho^2\frac{d\omega}{dt},$$

where: m is the total loaded mass of the robot platform, ρ is the radius of inertia of the mass m with respect to Z axis perpendicular to the xoy plane and passing through the center of mass; $\frac{d\omega}{dt}$ is the angular acceleration of the rotational motion of the robot platform during turning (for uniform motion $\frac{d\omega}{dt}=0$). G_y is the component of the gravitational force directed along the transverse axis of symmetry (y_2) of the platform:

$$G_y=G\cdot sin\beta\cdot sin\varphi.$$

N is the centrifugal force generated during turning motion:

$$N=m\omega^2R_0.$$

Let us determine the magnitude of the lateral drift forces for the adopted initial numerical values, when $\varphi=90^0$ and G_y attains its maximum value:

$$G_y=G\cdot sin\beta.$$

The numerical data are the same as in the previous example; in this case, the following additional data are also required:

$M_m=150N\cdot\text{m}$; $\eta=0.9$; $r_w=0.2m$; $Z_1=1004N$; $Z_2=1458N$; $Z_3=1458N$; $Z_4=1004N$; $\theta_1=12^0$; $\theta_2=9^0$; $\alpha=10^0$;

For these values, Equation (30) yields the following values for X_i. (assuming that the motion of the robot platform is uniform):

$X_1=349.0N$; $X_2=236.0N$; $X_3=236.0N$; $X_4=349.0N$.

Using Equation (32), the following value is obtained for M_z : $M_z=46.3N\cdot\text{m}$; $G_y=868N$; $N=193.25N$ (as noted earlier, in the considered case it is assumed that $M_j=0$).

Using Equations (33) and (34), the lateral drift forces ($Y_{\mathcal{A}}$ and Y_K) of the rear and front axles of the robotic platforms are obtained as:

$$Y_{\mathcal{A}}=568.0\ N;\ Y_K=508.8\ N.$$

For these values of lateral forces, lateral skidding will not occur provided that $(Z_3+Z_4)\cdot\mu>Y_{\mathcal{A}}$ and $(Z_1+Z_2)\cdot\mu>Y_K$, where μ is the coefficient of adhesion between the wheel and the supporting surface. For cultivated soil types $\mu=0{,}4\div 0{,}45$ (*Litvinov, 1971; Sineokov and Panov, 1977*). For the considered example:

$$(1004+1452)\cdot 0.45>Y_{\mathcal{A}}.$$

$$982.4\ N>\ 568.0\ N\text{, moreover,}$$

$$982.4\ N>\ 508.8\ N.$$

Therefore, the condition excluding lateral skidding is satisfied.

Evaluating and Ensuring the Smooth Motion of the Robot Platform

It is well established that, for mobile vehicles—including the robot platform considered and analyzed in this study—the maximum smoothness of motion is ensured when $a = \rho_1$, and in the present case, also when $b = \rho_2$ (*Litvinov,1971; Tarverdyan et al., 2025; Zinoviev, 1975*). Under these conditions, $\mathrm{M}_2 = 0$; $\mathrm{M}_4 = 0$ and therefore, Equations (25), (26), (27), (28) take the following form:

$$\mathrm{M}_1\left(\frac{d^2z_1}{dt^2}+\frac{d^2z_2}{dt^2}\right)+k\left(\frac{dz_1}{dt}+\frac{dz_4}{dt}\right)+c(z_1+z_4)=0, \tag{35}$$

$$\mathrm{M}_1\left(\frac{d^2z_3}{dt^2}+\frac{d^2z_4}{dt^2}\right)+k\left(\frac{dz_2}{dt}+\frac{dz_3}{dt}\right)+c(z_2+z_3)=0, \tag{36}$$

$$\mathrm{M}_3\left(\frac{d^2z_1}{dt^2}+\frac{d^2z_4}{dt^2}\right)+k\left(\frac{dz_1}{dt}+\frac{dz_2}{dt}\right)+c(z_1+z_2)=0, \tag{37}$$

$$\mathrm{M}_3\left(\frac{d^2z_2}{dt^2}+\frac{d^2z_3}{dt^2}\right)+k\left(\frac{dz_3}{dt}+\frac{dz_4}{dt}\right)+c(z_3+z_4)=0. \tag{38}$$

The following notations are introduced:

$$\left.\begin{array}{l} z_1+z_2=R; \\ z_1+z_4=Q; \\ z_3+z_4=F; \\ z_2+z_3=N; \end{array} \quad \text{and also note that } R+F=Q+N \right\} \tag{39}$$

Then, combining Equations (35) and (37) yields:

$$\begin{cases} \dfrac{d^2R}{dt^2}+\dfrac{k}{\mathrm{M}_1}\cdot\dfrac{dQ}{dt}+\dfrac{c}{\mathrm{M}_1}\cdot Q=0; \\ \dfrac{d^2Q}{dt^2}+\dfrac{k}{\mathrm{M}_1}\cdot\dfrac{dR}{dt}+\dfrac{c}{\mathrm{M}_1}\cdot R=0. \end{cases} \tag{40}$$

Similarly, from Equations (36) and (38):

$$\begin{cases} \dfrac{d^2F}{dt^2}+\dfrac{k}{\mathrm{M}_1}\cdot\dfrac{dN}{dt}+\dfrac{c}{\mathrm{M}_1}\cdot N=0; \\ \dfrac{d^2N}{dt^2}+\dfrac{k}{\mathrm{M}_3}\cdot\dfrac{dF}{dt}+\dfrac{c}{\mathrm{M}_3}\cdot F=0. \end{cases} \tag{41}$$

It follows from the latter equations that systems (40) and (41) are identical, i.e., $F = R$; $N = Q$. Therefore, it is sufficient to solve only system (40).

The following substitutions are introduced:

$$X=\sqrt{\mathrm{M}_1}\cdot R; \;\; Y=\sqrt{\mathrm{M}_3}\cdot Q \tag{42}$$

$$\alpha=\frac{k}{\sqrt{\mathrm{M}_1\cdot\mathrm{M}_3}}; \;\; \gamma=\frac{c}{\sqrt{\mathrm{M}_1\cdot\mathrm{M}_3}}. \tag{43}$$

The system of equations in Equation (40) can then be written as:

$$\begin{cases} X''+\alpha Y'+\gamma Y=0; \\ Y''+\alpha X'+\gamma Y=0. \end{cases} \tag{44}$$

The following notation is introduced:

$$X+Y=U; \;\; X-Y=V \tag{45}$$

Adding and subtracting the equations in system (44) yields:

$$U''+\alpha U'+\gamma U=0; \tag{46}$$

$$V''-\alpha V'-\gamma Y=0. \tag{47}$$

The characteristic equation associated with Equation (46) will be:

$\varepsilon^2+\alpha\varepsilon+\gamma=0$; whose roots are:

$\varepsilon_{1,2}=\frac{-\alpha\pm\sqrt{\alpha^2-4\gamma}}{2}=\frac{-\alpha\pm i\sqrt{4\gamma-\alpha^2}}{2}=-\frac{\alpha}{2}\pm\frac{i\omega}{2}$, where $\omega=\sqrt{4\gamma-\alpha^2}$.

Since $4\gamma>\alpha^2$, the general solution of Equation (46) will be:

$$U(t)=e^{-\frac{\alpha t}{2}}\left(\mathrm{A}_1 cos\frac{\omega}{2}t+\mathrm{A}_2 sin\frac{\omega}{2}t\right). \tag{48}$$

The characteristic equation associated with Equation (47) is: $\xi^2-\alpha\xi-\gamma=0$, which has two real roots:

$\varepsilon_{1,2}=\frac{\alpha\pm\sqrt{\alpha^2+4\gamma}}{2}$, besides $\varepsilon_1=\frac{\alpha+\sqrt{\alpha^2+4\gamma}}{2}>0$.

The general solution of Equation (47) is therefore:

$$V(t)=\mathrm{A}_3e^{\varepsilon_1 t}+\mathrm{A}_4e^{\varepsilon_2 t}. \tag{49}$$

Because an exponentially increasing solution has no physical meaning in this context, the following condition $A_3 = 0$ is imposed.

Returning to the original functions R and Q and using Equations (42) and (45), the following is obtained:

$$R = \frac{U+V}{2\sqrt{M_1}};\ Q = \frac{U-V}{2\sqrt{M_3}},\ \text{or}$$

$$R(t) = \frac{1}{2\sqrt{M_1}}\left[e^{-\frac{\alpha t}{2}}\left(A_1 cos\frac{\omega}{2}t + A_2 sin\frac{\omega}{2}t\right) + A_4 e^{\varepsilon_2 t}\right]; \tag{50}$$

$$Q(t) = \frac{1}{2\sqrt{M_3}}\left[e^{-\frac{\alpha t}{2}}\left(A_1 cos\frac{\omega}{2}t + A_2 sin\frac{\omega}{2}t\right) - A_4 e^{\varepsilon_2 t}\right]. \tag{51}$$

The solution to system (39) is now considered. Taking into account that $R + F = Q + N; \Rightarrow R = Q$, the solution can be expressed as:

$$z_1 = Q - z_4; \qquad z_2 = R - Q + z_4; \qquad z_3 = F - z_4.$$

where z_4 is an arbitrary function.

Using the geometric relationship among the vertical linear displacements given by Equation (14), the following expression is obtained:

$Q - z_4 + F - z_4 = R - Q + z_4 + z_4$, from which it follows that:

$$z_4 = \frac{2Q}{4} = \frac{Q}{2} = \frac{R}{2}.$$

Thus: $z_1 = z_2 = z_3 = z_4 = \frac{R}{2}$.

The initial conditions are: $\begin{cases} z_{i(0)} = \delta, & i = 1,2,3,4 \\ z'_{i(0)} = 0, & i = 1,2,3,4. \end{cases}$

Where δ is the static deflection of the elastic element (spring) of the suspension system under the static load.

$$\left.\begin{aligned} z_{1(0)} &= \frac{R(0)}{2} = \delta \Rightarrow \frac{1}{4\sqrt{M_1}}(A_1 + A_4) \\ z_{2(0)} &= \frac{Q(0)}{2} = \delta \Rightarrow \frac{1}{4\sqrt{M_3}}(A_1 - A_4) \end{aligned}\right\},\ \text{wherefrom}$$

$$\left.\begin{aligned} A_1 &= 2\delta\left(\sqrt{M_1} + \sqrt{M_3}\right) \\ A_4 &= 2\delta\left(\sqrt{M_1} - \sqrt{M_3}\right) \end{aligned}\right\} \tag{52}$$

The following condition is now applied: $z'_{i(0)} = 0,\ z'_{1(0)} = 0 = \frac{R'(0)}{2} = \frac{1}{4\sqrt{M_1}}\left(-\frac{\alpha}{2}A_1 + A_2\frac{\omega}{2} + A_4\varepsilon_2\right)$,

$$z'_{2(0)} = 0 = \frac{Q'(0)}{2} = \frac{1}{4\sqrt{M_3}}\left(-\frac{\alpha}{2}A_1 + A_2\frac{\omega}{2} - A_4\xi_2\right),$$

From the latter equations it follows that:

$$\begin{cases} A_2\frac{\omega}{2} = \frac{\alpha}{2}A_1 - A_4\varepsilon_2\,, \\ A_2\frac{\omega}{2} = A_4\varepsilon_2 + \frac{\alpha}{2}A_1, \end{cases}$$

from which it follows that:

$$A_4 = 0, \quad A_2 = \frac{\alpha A_1}{\omega} = \frac{2\delta\alpha}{\omega}\left(\sqrt{M_1} + \sqrt{M_3}\right). \tag{53}$$

From the condition $A_4 = 0$, it becomes evident that $\sqrt{M_1} = \sqrt{M_3}$, $M_1 = M_3$.

Thus, taking into account Equations (50), (51), (52) and (53), the following equation is obtained for the linear displacements of oscillation:

$$z_1 = z_2 = z_3 = z_4 = \frac{1}{4\sqrt{M_1}} \cdot e^{-\frac{\alpha t}{2}}\left(4\delta\sqrt{M_1} \cdot cos\frac{\omega t}{2} + \frac{4\delta\alpha}{\omega} \cdot \sqrt{M_1} sin\frac{\omega t}{2}\right).$$

Or, in final form:

$$z_{i(t)} = \delta e^{-\frac{\alpha t}{2}} \cdot \left(cos\frac{\omega t}{2} + \frac{\alpha}{\omega} \cdot sin\frac{\omega t}{2}\right) \tag{54}$$

Based on the analysis of the free oscillations of the robotic platform, the derived equations make it possible to determine the key oscillation parameters included in the characteristic performance indicators of the suspension system, namely the oscillation frequency, amplitude, and period, which determine the smoothness of motion (*Biderman, 1980; Ilarionov, 2013; Zinoviev,1975*). In addition, the final Equation (54) makes it possible to determine the oscillation velocity: $\left(\frac{dz}{dt}\right)$

The acceleration: $\left(\frac{d^2z}{dt^2}\right)$ and the rate of acceleration change, which is an important characteristic parameter in problems of this type: $\left(\frac{d^3z}{dt^3}\right)$.

Based on Equation (54), the equations derived from it, and the initial parameters of the robotic platform being developed, the following values were adopted: L=1,60 m; B=1,20 m; a=0,8 m; b=0,6 m; $\rho_1 = 0{,}8\ m$; $\rho_2 = 0{,}6\ m$; M=500 kg. Under these conditions: $\mathrm{M_1} = \mathrm{M_2} = \mathrm{M_3} = \mathrm{M_4} = 125\ \mathrm{kg}$, the equivalent stiffness coefficient of the suspension system is: $c_b = 66.65 \cdot 10^3 \frac{N}{m} = 66.65 \cdot 10^3 \frac{kg}{s^2}$, the average value of the resistance coefficient of a shock absorber: $k = 420 \frac{N \cdot s}{m} = 420 \frac{kg}{s}$, the vertical static deflection: $\delta = 0.01\ m$, and with calculated values: $\alpha = \frac{k}{M_1} = \frac{420}{125} = 3.36\ s^{-1}$, $\frac{\alpha}{2} = 1.68\ s^{-1}$, $\omega = \sqrt{\frac{4c}{M_1} - \alpha^2} = \sqrt{\frac{4 \cdot 66.65 \cdot 10^3}{125} - (3.36)^2} = 46.06 s^{-1}$, the graphs of the obtained functions are presented in Figure 7.

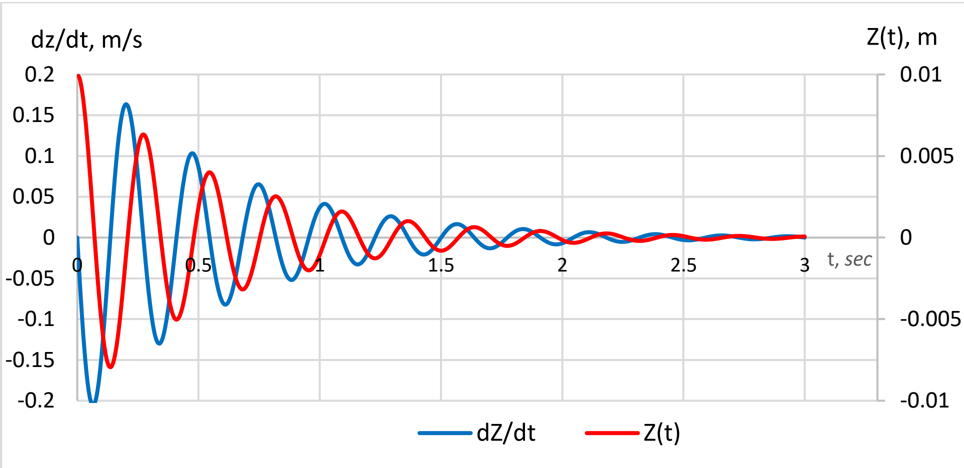

a)

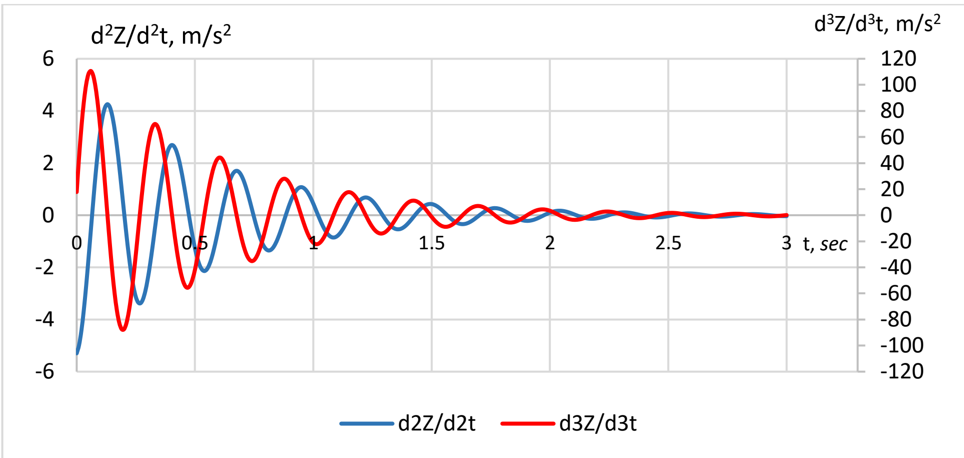

b)

Fig. 7 - Graphs of the free oscillations of the robot platform

a) vertical displacements and velocities; b) velocities and accelerations.

The obtained analytical equations make it possible to select such stiffness values (c) for the elastic elements of the suspension system and such a damping coefficient (k), for the shock absorber (damper) that the required programmed parameters of the oscillatory motion are ensured.

Furthermore, the presented results and derived equations provide the basis for the next stage of the research, namely the investigation of the forced oscillations of the robotic platform.

CONCLUSIONS

As a result of the stability analysis of the developed agricultural robotic platform equipped with four driven and self-steering wheels operating on slopes, analytical equations were obtained that make it possible to determine the conditions of rollover and sideslip during turning motion, as well as the threshold values of the slope angle and the linear velocity of turning motion.

The magnitude of the torque about the vertical axis, which is characteristic particularly of four-wheeled robotic platforms with self-steering wheels operating on slopes and has a significant influence on skidding phenomenon, was determined.

Based on the analysis of the differential equation describing the motion of the robotic platform's center of mass and the torque equations with respect to the platform's transverse and longitudinal symmetry axes, the equations of the robotic platform's free oscillations were derived. The derived equations make it possible to determine the vertical displacements, velocities, accelerations, and variations of acceleration of the oscillatory motion, as well as choosing the stiffness of the shock absorber (damper) required to ensure smooth motion of the platform.

The obtained results are of considerable significance and provide a foundation for further investigations into the forced vibration behavior of the robotic platform.

REFERENCES

[1] Abrosimov, V.K., Raykov, A.N. (2022). Intelligent Agricultural Robots (*Интеллектуальные сельскохозяйственные роботы*). Career Press (*Карьера Пррес*), Moscow, 512p.

[2] Akimov, A.V. (2017). Robotics and labor-saving technologies: perspectives of impact on socio-economic development (*Робототехника и трудосберегающие технологии: перспективы воздействия на социально-экономическое развитие*). Historical psychology and sociology (*Историческая психология и социология истории*). - No 1. - pp. 173-192.

[3] Ali, M.A., Kim, C., Kim, S. Khan A.M., Iqbal J, Khalil M.Z., Lim D. and Han Ch. (2017) Lateral acceleration potential field function control for rollover safety of multi-wheel military vehicle with in-wheel-motors. *Int. J. Control Autom. Syst.* 15, 837–847. https://doi.org/10.1007/s12555-014-0573-7

[4] Amin, A., Wang, X., Chen, Y., Guoxiang, S., Xuekai, H., Rottok, L.T., Sayed, H.A.A., Okasha, M. and Hassanien, R.H.E. (2025), Enhancing Greenhouse Performance Through Robotic Roof Cleaning Solutions: A Review. Journal of Field Robotics, 42: 1401-1426. https://doi.org/10.1002/rob.22459

[5] Bak T., Jakobsen H. (2004). Agricultural Robotic Platform with Four Wheel Steering for Weed Detection. *Biosystems Engineering* 87(2), 125-136, DOI:10.1016/j.biosystemseng.2003.10.009.

[6] Bayar, G., Bergerman, M., Koku, A. B., & Ilhan, Konukseven, E. (2015). Localization and control of an autonomous orchard vehicle, *Computers and Electronics in Agriculture*, Volume 115, , Pages 118-128, https://doi.org/10.1016/j.compag.2015.05.015

[7] Biderman V.A.(1980). Theory of Mechanical Oscillations (*Теория механических колебаний*), Mashinostroenie (*Машиностроение*), Moscow.

[8] Blasco, J., Aleixos, N., Rojer, J. M., Rabatal, G., Molto, E. (2002). Robotic weed control using machine vision. *Biosystems Engineering*, 83(2), 149-157.

[9] Buchholz N.N. (2023). Basic Course of Theoretical Mechanics, Part 1 and 2 (*Основной курс теоретической механики, часть 1 и 2*), Lomonosov Moscow State University Publishing House (*Издательство МГУ им. Ломоносова*), Moscow.

[10] Cho, S. I., Kim, Y.Y., An, K.J. (2002). Development of a three-degrees-of-freedom robot for harvesting lettuce using machine vision and fuzzy logic control. *Biosystems Engineering*, 82(2), 143-149.

[11] Fontani, M., Luglio, S. M., Gagliardi, L., Peruzzi, A., Frasconi, C., Raffaelli, M., & Fontanelli, M. (2025). A Systematic Review of 59 Field Robots for Agricultural Tasks: Applications, Trends, and Future Directions. *Agronomy*, 15(9), 2185. https://doi.org/10.3390/agronomy15092185

[12] Fountas, S., Mylonas, N., Malounas, I., Rodias, E., Hellmann Santos, C., & Pekkeriet, E., (2020). Agricultural Robotics for Field Operations. *Sensors*, *20*(9), 2672. https://doi.org/10.3390/s20092672

[13] Ilarionov V.A. (2013). Theory of Automobile (*Теория автомобиля*), NSTU Publishing House, (*Издателтство НГТУ*), Nizhny Novgorod.

[14] Ivanov R., Ivanova D., Kadikyanov G., Staneva G., Minkovska L. (2025) Theoretical study of the stability of a two-axle vehicle with a dynamic model. *Transport Problems,* 20(3):229-241. http://doi.org/10.20858/tp.2025.20.3.18

[15] Li Zhipeng, Shi Songzhuo (2017) Stability of eps system of agricultural vehicles under vibration environment. *INMATEH-Agricultural Engineering*, Vol.51, No.1, 101-110

[16] Lipiński Adam J., Markowski P., Lipiński S., Pyra P., (2016). Precision of tractor operations with soil cultivation implements using manual and automatic steering modes, *Biosystems Engineering,* Volume 145, Pages 22-28, ISSN 1537-5110, https://doi.org/10.1016/j.biosystemseng.2016.02.008.

[17] Litvinov, A.S. (1971). Automobile Controllability and Stability (*Управляемость и устойчивость автомобиля*). Mashinostroenie (*Машиностроение*). Moscow, - 416p.

[18] MarketsandMarkets. (2025, November 7). *Agricultural robots market by robot type, application, offering, end use, farming environment, farm size, and region – global forecast to 2030*. https://www.marketsandmarkets.com/Market-Reports/agricultural-robot-market-173601759.html

[19] Navone A., Martini M., Chiaberge M., (2025). Autonomous robotic pruning in orchards and vineyards: A review, *Smart Agricultural Technology*, Volume 12, 101283, ISSN 2772-3755, https://doi.org/10.1016/j.atech.2025.101283.

[20] O'Meara P. (2019). The ageing farming workforce and the health and sustainability of agricultural communities: A narrative review. *Aust J Rural Health*; 27: 281–289. https://doi.org/10.1111/ajr.12543

[21] Orebäck A; Christensen, H. I. (2003). Evaluation of architectures for mobile robotics. *Autonomous Robots*, 14(1), 33-49.

[22] Qiu Q., Fan Z., Meng Zh., Zhang Q., Cong Y., Li B., Wang N., Zhao Ch., (2018). Extended Ackerman Steering Principle for the coordinated movement control of a four wheel drive agricultural mobile robot, *Computers and Electronics in Agriculture*, Volume 152, Pages 40-50, ISSN 0168-1699, https://doi.org/10.1016/j.compag.2018.06.036.

[23] Ritchie H. (2019). Food production is responsible for one-quarter of the world's greenhouse gas emissions, *Published online at OurWorldinData.org. Retrieved from: https://archive.ourworldindata.org/20251125-173858/food-ghg-emissions.html [Online Resource] (archived on November 25, 2025).*

[24] Sineokov G.N., Panov I.M., (1977) *Theory and calculation of tillage machines (Теория и расчет почвообрабатывающих машин)*, Mashinostroenie (Машиностроение), Moscow -322 p.

[25] Tarverdyan, A., Altunyan, A., Grigoryan, A., (2025). Justification of the Kinematic Parameters of the Running Gear of a Horticultural Robot Platform. "*Agriscience and Technology*", International scientific journal, Armenian National Agrarian University, - №2(90), - pp. 112-119. https://doi.org/10.52276/25792822-2025.2-112

[26] Torii, T. (2000). Research in autonomous agriculture vehicles in Japan. *Computers and Electronics in Agriculture*, 25 (1-2),-pp. 133-153. https://doi.org/0.1016/S0168-1699(99)00060-5

[27] Zagazezheva, O.Z., Berbekova, M.M. (2021). The main trends in the development of robotic technologies in agriculture. *News of the Kabardino-Balkarian Scientific Center of RAS*. - No.5 (103), - pp. 11-20. https://doi.org/10.35330/1991-6639-2021-5-103-11-20.

[28] Zakaria, M.S.M., Singh, A.S.P. and Aras, M.S.M. (2024) "Integrated Chassis Control for Multi-Axle Vehicles: A Comprehensive Review", *International Journal of Automotive and Mechanical Engineering*, 21(3), pp. 11663–11681. doi:10.15282/ijame.21.3.2024.17.0900.

[29] Zinoviev V.A. (1975). *Theory of Mechanisms and Machines* (*Теория механизмов и машин*), Nauka (*Наука*), Moscow.